7884–7900 *Nucleic Acids Research, 2021, Vol. 49, No. 14* *Published online 21 July 2021*
https://doi.org/10.1093/nar/gkab611

Stabilization and structural changes of 2D DNA origami by enzymatic ligation

Arivazhagan Rajendran †, Kirankumar Krishnamurthy †, Amulya Giridasappa, Eiji Nakata and Takashi Morii *

Institute of Advanced Energy, Kyoto University, Gokasho, Uji, Kyoto 611-0011, Japan

Received March 03, 2021; Revised June 16, 2021; Editorial Decision July 01, 2021; Accepted July 06, 2021

ABSTRACT

The low thermal stability of DNA nanostructures is the major drawback in their practical applications. Most of the DNA nanotubes/tiles and the DNA origami structures melt below 60°C due to the presence of discontinuities in the phosphate backbone (i.e., nicks) of the staple strands. In molecular biology, enzymatic ligation is commonly used to seal the nicks in the duplex DNA. However, in DNA nanotechnology, the ligation procedures are neither optimized for the DNA origami nor routinely applied to link the nicks in it. Here, we report a detailed analysis and optimization of the conditions for the enzymatic ligation of the staple strands in four types of 2D square lattice DNA origami. Our results indicated that the ligation takes overnight, efficient at 37°C rather than the usual 16°C or room temperature, and typically requires much higher concentration of T4 DNA ligase. Under the optimized conditions, up to 10 staples ligation with a maximum ligation efficiency of 55% was achieved. Also, the ligation is found to increase the thermal stability of the origami as low as 5°C to as high as 20°C, depending on the structure. Further, our studies indicated that the ligation of the staple strands influences the globular structure/planarity of the DNA origami, and the origami is more compact when the staples are ligated. The globular structure of the native and ligated origami was also found to be altered dynamically and progressively upon ethidium bromide intercalation in a concentration-dependent manner.

INTRODUCTION

The structural DNA nanotechnology (1,2) has attracted much attention during the past one and a half decades due to the addition of the scaffolded DNA origami method (3) to the field. This method has enabled the synthesis of DNA nanostructures with the dimension of ∼100 nm in diameter, whereas the initially prepared non-scaffolded structures were ∼10–20 nm in size (4–6). Since the invention of scaffolded origami, various two- (2D) (3) and three-dimensional (3D) (7–9) DNA origami have been synthesized, and also self-assembled further to create even larger structures (10–13). The formation of DNA origami can also be controlled by using the external signals such as cationic comb-type copolymers/polyvinyl sulphonic acid (14) and DNA-binding dendrons/reducing agents or light (15). Origami materials can also be lyophilized and stored for future applications (16). These structures have been used as novel scaffolds for nanopatterning of various nanoparticles (17,18) and quantum dots (19), attachment of carbon nanotubes (20), immobilization of biomolecules such as proteins (21) and viral capsids (22), carriers of drugs (23), platform for the analysis of single molecular reactions and processes (24), and so on.

One major issue with these nano-biomaterials is their unsatisfactory stability that prevents them from the applications in a wide range of conditions to withstand the thermal, mechanical and chemical modifications. For instance, the DNA origami structures that use most of the staples of length 32 bases melt below 60°C (25). Similar to the non-scaffolded DNA tube (26), the 3D DNA origami structures such as cuboid may also break open when deposited on mica or scanned by force-based methods (27) such as atomic force microscopy (AFM) (28), and also disintegrate in deionized water (26,29). As recently reviewed (30,31), several strategies have been employed to improve the stability of origami under application-specific conditions. These included the protective coatings, encapsulation of origami in protective shells, covalent modifications of DNA strands, and alterations in DNA phosphate backbone. One major reason for the stability issues of the origami structures is the presence of breaks in the phosphate backbone, the so-called nicks, in the staple strands. For example, a typical

*To whom correspondence should be addressed. Tel: +81 774 38 3585; Fax: +81 774 38 3516; Email: t-morii@iae.kyoto-u.ac.jp
†The authors wish it to be known that, in their opinion, the first two authors should be regarded as Joint First Authors.
Present address: Amulya Giridasappa, Department of Nanotechnology, Visvesvaraya Technological University, Muddenahalli, Chikkaballapur, Karnataka 562 101, India.

2D DNA origami synthesized using 226 staples contains the same number of nicks in the phosphate backbone. Increasing the staple length would improve the thermal stability, but at the same time will lead to practical difficulties such as increased cost of synthesis, decreased product yield and purity, and limitations on the maximum length of synthetic oligo DNAs.

We have previously reported a method to stabilize the DNA origami structures by photo-cross-linking of 8-methoxypsoralen (8-MOP), found in a variety of vegetables and it is a commonly used drug to treat dermatoses, by UVA irradiation (25). Another method is the UVB light-induced cyclobutane pyrimidine dimer (CPD) formation by placing thymidines in a close proximity within DNA origami (29). The advantage with our method is the long wavelength UVA treatment (25) which neither induces DNA lesions nor significantly damages the DNA origami structure even at doses of 200 kJ/m^2 (32). Whereas, UVB and UVC irradiations lead to the formation of CPD and degrade the origami even at the low radiation doses of 20.3 and 8.3 kJ/m^2, respectively (32). Despite their advantages, these methods are not suitable where native-like DNA is anticipated, as they introduce chemical cross-links to the DNA strands. The alternative method is the enzymatic ligation of the nicks, the method that is routinely used in molecular biology. Enzymatic ligation was also applied for the small DNA nanostructures such as the DNA nanotubes with the size of ∼10 nm in diameter that contains only five nicks (26) or only two sticky ends (33), DNA triangles containing double crossover molecules (34), four-arm DNA junctions (35), and the DNA triple crossover complexes (36). Among these structures, the short DNA nanotube was ligated with the average efficiency of 68–77% (26), while no ligation yield was reported for other structures. Also, enzymatic ligation is not widely applied for the scaffolded DNA origami. There are only few reports exist in which the enzymatic ligation was carried out on DNA origami without optimizing the conditions (20,37–41). For example, a ligated rectangular DNA origami was used to encapsulate a virus capsid protein (CP) and further used for the cellular delivery (38). The other reports in which the origami was ligated include the evaluation of origami staple redesign (37), self-assembly of carbon nanotubes on origami (20,39), the dielectrophoretic trapping (40), and the AC impedance spectroscopic analysis of origami (41). But, in all these reports, the ligation was not characterized and no evidence was provided to support the success of the enzymatic ligation on origami. DNA origami structure is a bundle of tightly packed anti-parallelly oriented multiple duplexes, and thus, the enzymatic ligation on that is expected to be very different from that of a simple duplex DNA or non-scaffolded DNA nanostructures consisting of relatively few ssDNAs (26,33–36). Crystal structures of ligases suggest that the enzymes completely encircle the nicked DNA to ligate the nick (42). The tightly packed DNA origami may restrict the access to the ligase, and thus, optimization of the conditions and well characterization of the ligation are necessary.

Here, we report a detailed characterization of the ligation of staple strand nicks in DNA origami carried out by T4 DNA ligase to establish optimized conditions for DNA nanostructures. In addition, the structural changes caused by the ligation of staples, and also the intercalator ethidium bromide (EtBr)-induced dynamic and progressive conformational changes in native and ligated origami were evaluated. The investigation on the access of the nick sites to the ligase enzyme and the ligation reaction in a tightly packed environment, such as the one in DNA origami, would provide a new insight on the structural features of origami from the mechanistic aspect of ligase reaction.

MATERIALS AND METHODS

Materials

Reagents for buffers such as tris(hydroxymethyl)aminom ethane (Tris-base), ethylenediaminetetraacetic acid disodium salt (EDTA.2Na), HCl, acetic acid, boric acid, NaCl and $MgCl_2$, and materials for the gel electrophoresis such as EtBr, agarose, acrylamide (monomer), N,N'-methylenebisacrylamide, ammonium persulfate (APS), and *N*,*N*,*N*',*N*'-tetramethylethane-1,2-diamine (TEMED) were purchased from Nacalai Tesque, Inc. (Kyoto, Japan). Adenosine triphosphate (cold ATP) was obtained from Sigma Aldrich (USA). The γ-^{32}P-ATP (hot ATP, stock concentration 1.66 μM, 10 mCi/ml) was received from PerkinElmer. T4 polynucleotide kinase (PNK) was purchased from TaKaRa Bio (Kyoto, Japan). Single-stranded M13mp18 viral DNA was received from Guild Biosciences (Dublin, USA). T4 DNA ligase was obtained from New England Biolabs Inc. (Ipswich, MA). The staple strands for the preparation of DNA origami were purchased from ThermoFisher Scientific (Tokyo, Japan). Proteinase K was received from Wako Pure Chemical Industries, Ltd. (Osaka, Japan). The empty gel-filtration column (to pack S-300 or S-400) and Micro Bio-Spin 6 column were obtained from Bio-Rad Laboratories Inc. (Hercules, CA). Sephacryl S-300 and S-400 were purchased from GE Healthcare UK Ltd. (Buckinghamshire, UK). All the chemicals and reagents used were molecular biology grade. Water was deionized (specific resistance >18.0 MΩ cm at 25°C) using a Milli-Q system (Millipore Corp., Bedford, MA).

Design of DNA origami

As shown in Figure 1 (and Supplementary information Figures S1–S4), we have adapted four different DNA origami, namely rectangle (Rec) (3), and 1 (1WF) (43), 3 (3WF) (44) and 5 well frame (5WF) (45) origami. The theoretical dimensions are 98 × 83 nm, 98 × 111 nm, 141 × 76 nm, and 98 × 111 nm respectively for Rec, 1WF, 3WF and 5WF. The choice of these 2D origami structures is based on the following facts: (i) in the frame-shaped origami, the ligase may have more access when the number of wells is increased, while it is possibly reduced in the rectangle origami. Thus, the access-dependent ligation can be probed and (ii) the length of the staple strands is mostly 32 nucleotides in Rec and 1WF, while longer in 3WF (up to 64 nucleotides) and 5WF (up to 72 nucleotides, see Figure 1B). Therefore, the staple length-dependent ligation and structural changes in DNA origami can be probed. Note that the number of staples indicates the number of nick sites in each origami.

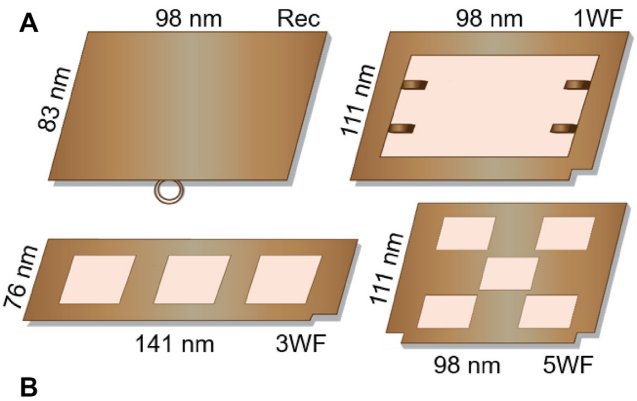

B

Staple length (bases)	Number of staples				Staple length (bases)	Number of staples			
	Rec	1WF	3WF	5WF		Rec	1WF	3WF	5WF
23			1		44		2		1
24		4			46			4	
26	6				47			7	
27	4				48	2		17	18
28	2				49			1	
30			3		54			2	
31			98		56				12
32	192	170	42	64	60				2
34		18			61			1	
36	20	29			62			1	
38			2		64			1	34
39			10		72				12
40		3	9	16	Total	226	226	199	159
Above 32 mer	22	52	65	95	Max. length	48	44	64	72

Figure 1. (**A**) Schematic outline of the rectangle (Rec), 1 (1WF), 3 (3WF), and 5 well frame (5WF) origami that are used in this study. The dimension of each origami is given. (**B**) Length distribution of the staple strands of all the four origami. The number of staples above the length of 32 bases, maximum length, and total number of the staple strands are indicated in each case.

Buffer conditions

1× PNK buffer: 50 mM Tris–HCl, 10 mM $MgCl_2$ and 5 mM DTT (pH 7.5). 1× origami buffer: 40 mM Tris-base, 20 mM acetic acid, and 12.5 mM $MgCl_2$ (pH 8.2).

Annealing conditions

PNK reactions were carried out at 37°C for 30 min, denatured at 70°C for 10 min, and then rapidly cooled down to 4°C. For DNA origami preparation, the solutions were incubated at 95°C for 1 min, rapidly cooled down to 53°C, incubated for 30 min, and finally rapidly cooled down to 4°C. For ligase reactions, the solutions were incubated overnight (or as indicated) at 4, 16°C, room temperature (RT), 37, 42 or 47°C.

Confirmation of phosphorylation

The synthetic staple strand oligomer DNAs lack the 5′-phosphate that is necessary for the ligation. Thus, before the ligation reaction, it is necessary to phosphorylate the staple strands. Prior to the kinase reaction, all the staple strands used in this study were buffer exchanged into Tris–HCl (10 mM, pH 7.5) containing NaCl (20 mM) by using Micro Bio-Spin 6 column to get rid of the kinase inhibitors such as ammonium and phosphate salts. The 5′-phosphorylation was performed by using a mixture of 1WF staple strands and γ-^{32}P-labelled ATP. For this purpose, a mixture of non-labelled cold ATP and γ-^{32}P-labelled hot ATP were used in a ratio of 10 000:1, respectively. In our case, a typical DNA origami synthesis of 10 nM concentration requires 4-times higher amount of the mixture of staple strands, i.e. 10 nM × 4-times × 226 staples = ∼9 μM of total strand concentration. Both 1:1 (i.e. each 9 μM) and 1:2 ratio of staple strands:ATP mixture were tested using 5–30 U of PNK. In typical reactions, the staple strands and ATP mixtures were taken in 1× PNK buffer. The indicated amount of PNK was added to the reaction mixtures and the reaction was carried out by following the PNK annealing conditions mentioned above. The samples were then analyzed by 15% denaturing polyacrylamide gel electrophoresis (PAGE) as described below.

Enzymatic ligation

At first, the staple strands were phosphorylated at the 5′-end as described above. In a typical origami synthesis of 30 nM, we have taken the mixture of staple strands (120 nM of each strand) in 1× PNK buffer that contained 54 μM of ATP (1:2 ratio of staple:ATP). Though 10 U of PNK is sufficient (estimated for 10 nM origami synthesis), 20 U of PNK was constantly used to ensure the complete reaction. The PNK reaction was carried out as described above. M13mp18 ssDNA (30 nM) was then added to the reaction mixture and annealed the solution from 95 to 4°C. After the origami folding, the solution was purified (to get rid of the excess staples and PNK) and buffer exchanged into Tris–HCl (10 mM, pH 7.5) containing NaCl (20 mM) by using sephacryl S-300 (Rec, 1WF and 3WF) or S-400 (5WF) gel filtration columns. The absorption of purified DNA origami was then measured by NanoDrop-2000 spectrophotometer (ThermoFisher Scientific), and the concentration was calculated using the estimated molar absorption coefficient of the origami at 260 nm ($\varepsilon = 12.4 \times 10^7\ M^{-1}\ cm^{-1}$). From the known concentration of purified sample, 15 nM of DNA origami was taken in 1× PNK buffer (Note: We used the same buffer for both PNK and ligase reactions as their composition is the same) that contained 0.5 mM ATP (unless otherwise noted in specific cases). T4 DNA ligase (400–4800 U, as indicated in each case) was added to the ligation reaction mixture, and then incubated overnight (or as indicated) at the mentioned temperature. For comparison, the non-ligated origami was also prepared and treated under similar conditions but without ligase. After the ligation reaction, 40 nM of the non-phosphorylated staple strands were added to the reaction mixture (necessary for better recovery of DNA origami), and purified and buffer exchanged into 1× origami buffer by using sephacryl column. The purified samples were quantified once again by using NanoDrop. Once the phosphorylation and ligation were optimized, the following optimized conditions were used for any further analysis: PNK reaction: 1× PNK buffer, 1:2 ratio of staple:ATP, 20 U of PNK, and 37°C for 30 min. Ligase reaction: 1× PNK buffer, 0.5 mM of ATP, 15 nM (or as men-

tioned) of purified origami, 2400 U of ligase, and overnight incubation at 37°C. Note that the kinase and ligase reactions were carried out in a reaction volume of 50 μl, and the concentration of enzymes in unit (U) is related to this volume.

UV-melting analysis

UV-visible spectrophotometer (UV-1700 PharmaSpec, Shimadzu) was used to measure the melting patterns of the non-ligated and ligated origami samples. Typically, a 4 nM (100 μl) of the purified sample was taken in 1× origami buffer. The 8 series micro multi-cell (10 mm path length) was used for the parallel analysis of multiple samples. The 1× origami buffer was used for the blank correction. The melting was carried out from 25 to 95°C with the heating rate of 0.5°C/min, and the data was collected at every 0.5°C. The obtained melting curves were analysed using OriginPro 2020 software. The hypochromicity values were calculated using the following equation: % hypochromicity = $[(A_{\text{Native}} - A_{\text{Ligated}})/A_{\text{Native}}] \times 100$, where A_{Native} and A_{Ligated} are the absorbance of the native and ligated origami at 260 nm, respectively.

Native agarose gel electrophoresis (AGE)

Typically, a 3 nM (final concentration) of origami was mixed with orange G (final concentration of 1×) and loaded into a 1% agarose gel. The gel was run by using 1× TBE running buffer at 100 V and 4°C. The gels were then stained using EtBr in 1× TBE for 30 min, and the images were recorded on a Pharos FX Molecular Imager (Bio-Rad). Proteinase K treatment (Figure 5B): After the ligation reaction, Proteinase K (10 μg) was added into the samples and incubated at 37°C for 1 h. Then the reaction mixture was purified by using sephacryl S-300 and buffer exchanged into 1× origami buffer. The AGE analysis was then performed as described above. Only for the experiments in Figure 7A–D bottom panels, EtBr (0.5 or 1 μg/ml) was added both to the gel and running buffer prior to the gel running. For the experiments presented in Figure 8, the indicated amount of EtBr was added to each sample before loading them into the gel. The relative retention factor (R_f) of each band in the AGE was calculated in reference to the relative migration of the non-ligated native origami from the sample loading well, by using the following equation: $R_f = (L_{\text{Ligated}} - L_{\text{Native}})/L_{\text{Native}}$, where, L_{Ligated} and L_{Native} are the length of migration of the ligated and native origami bands, respectively from the sample loading wells. Only for Figure 7: R_f calculations were in reference with the migration of the native Rec.

Denaturing PAGE

EtBr staining: The samples were freeze-dried on a lyophilizer (Asahi Life Science), dissolved in Milli Q water, and formamide was added to the final concentration of 80–90% (v/v). Then the samples were denatured at 95°C for 10 min and rapidly cooled down on ice. The denatured samples were then loaded into a 12% PAGE containing 8 M urea. Low molecular weight DNA ladder (NEB, England) was also denatured similarly (without lyophilization) and loaded into the gels. The gels were run by using 1× TBE running buffer at 150 V and RT. The gels were then stained using EtBr in 1× TBE for 20 min, and the images were recorded on a Pharos FX Molecular Imager. ^{32}P-labelled experiments: The ^{32}P-labelled experiments were carried out similarly as mentioned above, except that a mixture of hot and cold ATPs was used for the PNK reaction. The lyophilization step was not carried out as the signal from 5′-^{32}P-staples was sufficient to detect. EtBr staining was not performed as it is unnecessary. The gels were imaged on a Storm 860 Molecular Imager (Amersham).

AFM imaging

AFM images were recorded using a Sample Scanning-Nano Explorer AFM system (SS-NEX, RIBM, Tsukuba) with a silicon nitride cantilever (resonant frequency: 1.5 MHz, spring constant: 0.1 N/m, Olympus) under the tapping mode. Before imaging, the samples were purified [to get rid of the ligase, ATP, and staple strands (if any)] and buffer-exchanged into 1× origami buffer using sephacryl column. Then, the purified samples were incubated discretely from 25 to 90°C for 10 min, and rapidly cooled down and stored on ice until AFM images were recorded. A 2 μl of sample (1–2 nM) was incubated on a freshly cleaved mica surface (ϕ 1.5 mm) for 5 min at RT, the surface was gently washed using 1× origami buffer, and images were recorded in the same buffer.

RESULTS

Phosphorylation of staple strands

At first, we have characterized the 5′-phosphorylation of the staple strands. This is necessary because incomplete phosphorylation was hypothetically reasoned for the incomplete ligation of non-scaffolded DNA nanotubes in a previous study (26). The phosphorylation was carried out by using PNK and the mixture of 1WF staple strands. The results indicated that a 30 min reaction was incomplete with 5 U of PNK, while the reaction goes to completion with 10–30 U of PNK (Figure 2A). Further, the reactions with double the amount of ATP indicated that there is no back reaction, i.e. from 5′-^{32}P-staples into inorganic phosphate (^{32}Pi), as the amount of the ^{32}Pi produced (∼10%) as a result of the degradation of γ-^{32}P-ATP was constant (Figure 2B). Though 10 U of PNK is sufficient, here after, 20 U of PNK was constantly used for any further experiments, as in some cases we needed to prepare higher amounts of up to 8-fold of DNA origami.

Optimization of enzymatic ligation in DNA origami

We then performed the enzymatic ligation of the 1WF origami and characterized the ligation by thermal melting using an UV–visible spectrophotometer. Initially, the ligase concentration-dependent analysis was carried out by the overnight ligation at 4°C. As shown in Figure 3A, the native origami started to melt at ∼56°C and the melting was saturated at ∼80°C. Due to the presence of 226 staples with different sequences and lengths (most of them

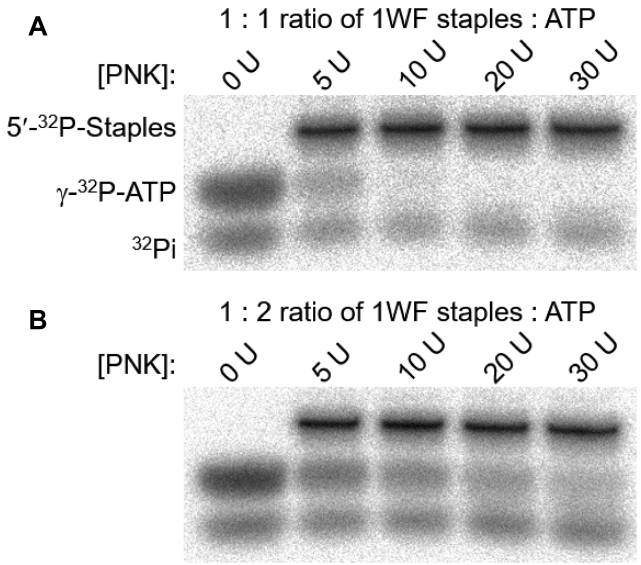

Figure 2. Denaturing PAGE images of the characterization of 5′-phosphorylation of the mixture of 1WF staple strands by using γ-^{32}P-ATP and PNK. The 1:1 (**A**) and 1:2 (**B**) ratio of staples:ATP were used for the reactions. The appearance of inorganic phosphate (^{32}Pi) is due to the decomposition of γ-^{32}P-ATP. [Staple strands] = 9 μM (total strand concentration); [Cold ATP] = 9 μM (for 1:1 ratio) or 18 μM (for 1:2 ratio); [Hot ATP] = 0.0009 μM (1:1 ratio) or 0.0018 μM (for 1:2 ratio); [PNK] = 0–30 U; [PNK buffer] = 1×, pH 7.5; PNK reaction: 37°C for 30 min; PNK denaturation: 70°C for 10 min; Denaturing PAGE: 8 M urea, 15% PAGE, 1× TBE running buffer, 100 V and ran at RT.

are 32 bases, but not all are the same in length, see Figure 1B), the 1WF melting curve exhibited multiple transitions that are hard to disintegrate. Thus, estimation of the exact or a single melting point is not possible, while there are at least two phases with the melting points roughly estimated at ∼60 and ∼64.5°C (see Supplementary Figures S5–S7 and Supplementary Table S1 for a detailed analysis of melting points). This observation is consistent with our previous study by using a jigsaw-shaped origami tile (25). Irrespective of the ligase concentration, the ligated origami also started to melt at the same temperature (∼56°C) with that of the native origami. However, no distinct saturation point of the melting was observed at higher temperature, and thus, the estimation of the accurate melting point is difficult. Interestingly, above 60°C, all the ligated samples exhibited hypochromicity when compared to the absorbance of native origami, and such a hypochromicity was maintained until the maximum tested melting temperature of 95°C. Further, the hypochromicity was more pronounced when the amount of ligase was increased from 400 to 2400 U, while slight increase in the absorbance was observed for the ligase concentrations of 3600 and 4800 U. The hypochromicities were highest at ∼77°C and the maximum hypochromicity of ∼39% was observed for 2400 U of ligase (see Figure 3A). A complete ligation would result in a distinct increase in the melting point, and its absence indicates that the ligation is incomplete. The observed hypochromicity further indicates that the ligation yield was not 100%, and thus, possibly the staples with various lengths are present in the semi-ligated origami. Due to the wide distribution of the staple lengths, the shorter staples such as the non-ligated 32-mer melts at lower temperature of ∼56–65°C, while the ligated longer staples melt at relatively higher temperatures. This leads to a continuous melting without a distinct transition and saturation point, and possibly, the longer staples (over 100-mer) was difficult to fully melt even until the maximum tested temperature of 95°C. This heterogeneous multi-state melting collectively leads to the observed hypochromicity. These results clearly indicate that the absolute and distinct melting point commonly observed with two-state systems is not a good measure of the ligation of DNA origami that follows multi-state melting, while the hypochromicity is a better indication of the ligation. From the above-mentioned observations, the ligase concentration of 2400–3600 U seems to be optimum.

The ligase concentration-dependent analyses were also carried out at RT and 37°C (all overnight reactions, Figure 3B, C). Similar melting patterns with that of the ligation at 4°C were observed in these higher temperature ligations. The hypochromicity was more pronounced for the ligation at RT and 37°C, when compared to the 4°C ligation (Figure 3A–C). Irrespective of the ligation temperature, the ligation seems to be saturating between the ligase concentrations of 2400–3600 U. A slight increase in the absorbance was observed with the ligase concentration of 4800 U. This small increase might have originated from the trace of enzyme remaining in the sample after the gel filtration particularly when the enzyme concentration is different. Also, this increase in absorbance was in the range of 0.008–0.011 which falls within the sensitivity of the UV-visible spectrophotometer, and thus, this small difference cannot be treated quantitatively. Alternative reasons of the ligation-induced structural changes in origami (as discussed below) and light scattering during UV-visible measurements are unlikely, and are not reasonable to expect only in the case of 4800 U of ligase. In addition to the hypochromicity, the melting point of the lower melting phase between 56 and 65°C (Figure 3A–C, indicated by horizontal arrow) was keep increasing when the ligation temperature was increased from 4 to 37°C. This is an additional indication that the ligation proceeds with higher efficiencies at higher temperature, as a result, the amount of 32-mer staples is decreasing and the ligated staples are melting at a relatively higher temperature.

AGE analyses of ligated 1WF

Along with the UV-melting analysis, an aliquot of each sample was taken and analyzed by means of the native AGE. From the AGE analysis, it is clear that the native 1WF migrates slower than the M13mp18, while the ligated samples migrate faster than the native origami (Figure 3D–F). Irrespective of the ligation temperature, the relative migration depends on the amount of ligase with the higher the amount of the ligase the faster the migration that was observed. Above the ligase concentration of 2400 U, only a slight increase in migration was observed, indicating that the ligation saturates around this enzyme concentration. The AGE data correlates well with the UV-melting analyses, and relative migration of the bands indicates the relative yield of the ligation, i.e. the faster migration of a band

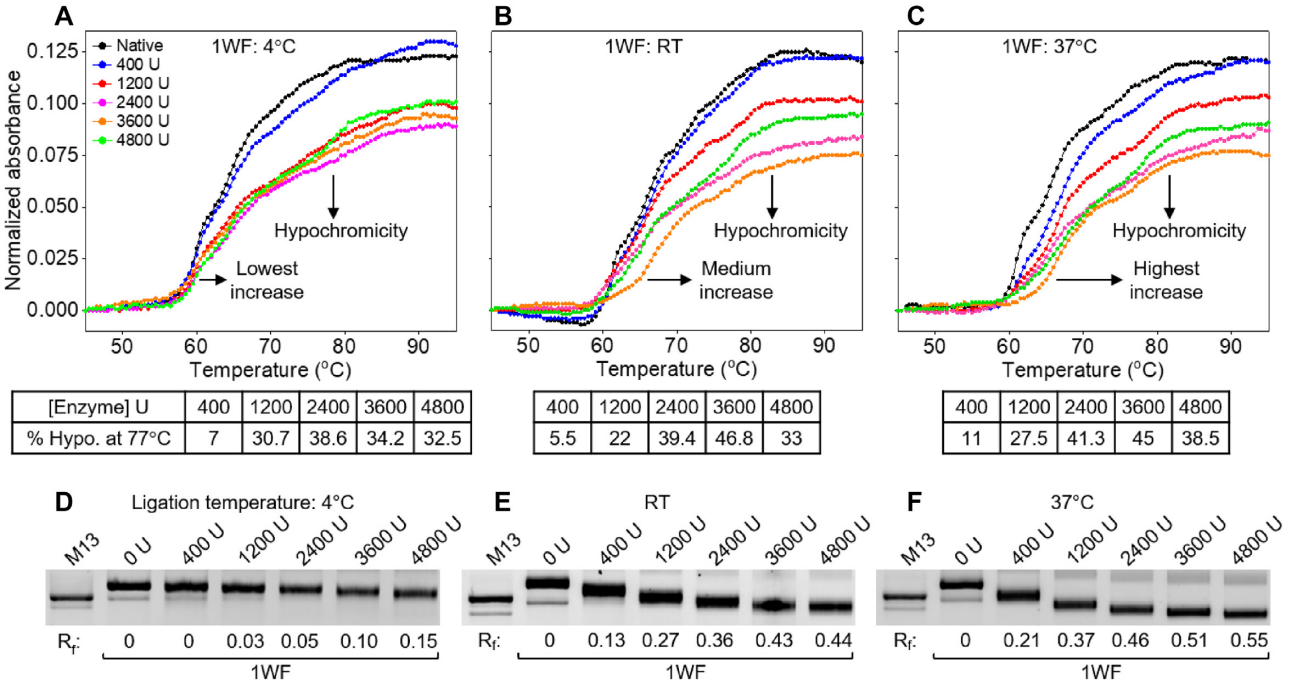

Figure 3. UV-melting analysis (top panel) and native AGE (bottom panel) of the native and ligated 1WF origami. The ligase concentration-dependent studies at 4°C (**A**, **D**), RT (**B**, **E**), and 37°C (**C**, **F**) are shown. The y-axis label and the colour schemes are the same for A–C. The estimated % hypochromicity at 77°C are tabulated below the UV-melting curves. The estimated R_f values are given below the AGE images. [1WF origami] = 4 nM (UV-melting) and 3 nM (AGE); ligation reaction time = overnight; Native AGE: 1% agarose, 1× TBE, 100 V, and ran at 4°C.

means a better ligation efficiency. The R_f values were estimated and listed below each AGE image. The highest R_f values were obtained for the ligation temperature of 37°C in which the ligated bands migrated even faster than the M13 (Figure 3F).

Analysis of ligation at various temperatures

In addition to the above-mentioned ligation temperatures, the ligation was also carried out at 16°C, and higher temperatures such as 42 and 47°C. As shown in Figure 4A, the maximum hypochromicity was observed for 37°C. The absorbance was significantly increased when we increased the ligation temperature any further and resulted the hypochromicity of ∼28 and 24% for the ligation temperatures of 42 and 47°C, respectively. The AGE analysis in Figure 4B also indicated that the maximum R_f of 0.51 was obtained for the ligation temperature of 37°C, and after such a temperature, the 1WF exhibited relatively slower migration. Based on these observations, we concluded that the ligation temperature of 37°C is optimum. At a relatively higher temperature of 37°C, the origami structure is possibly loosened and the nicks in the staples may be optimally exposed to the ligase to access and react. Hence, this leads to a better ligation efficiency than the ligation at relatively lower temperature of 4, 16°C and RT. The alternative reason for the optimum ligation temperature of 37°C could be the enzyme having its maximum activity at this temperature (46). At the ligation temperatures of 42 and 47°C, the ligase may be less stable that in turn leads to the relatively lower ligation efficiency. The previous report on the reduc-

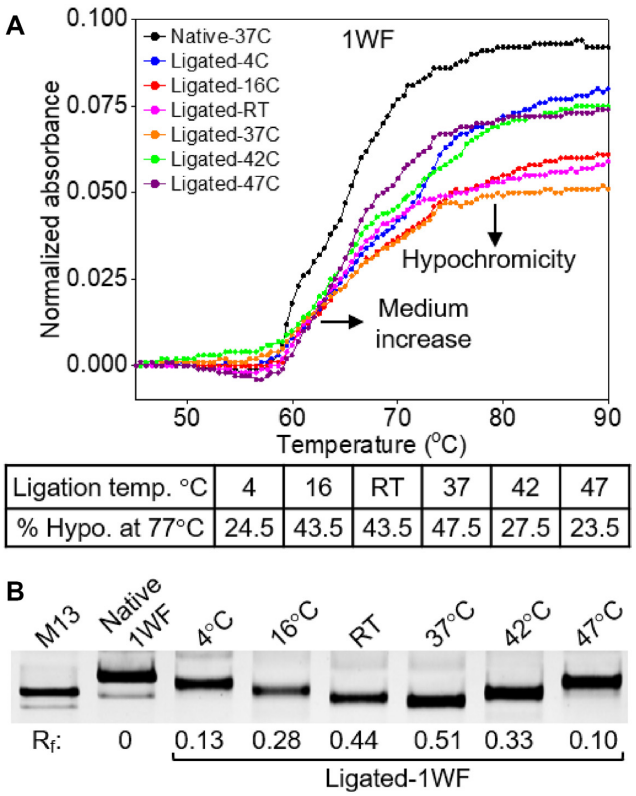

Figure 4. Effect of ligation temperature analyzed by UV-melting analysis (**A**) and native AGE (**B**). [1WF origami] = 4 nM (UV-melting) and 3 nM (AGE); [Ligase] = 2400 U; ligation reaction time = overnight.

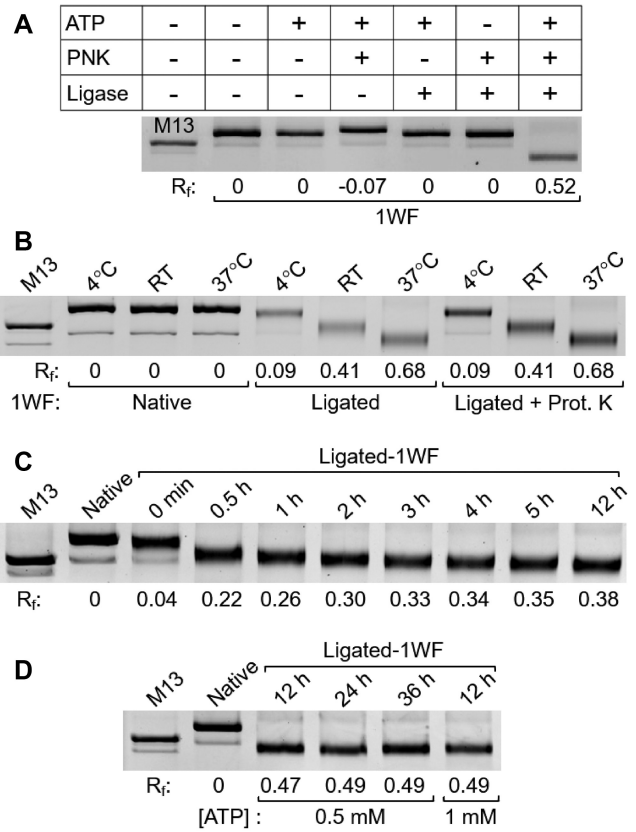

Figure 5. Native AGE images of the non-ligated and enzymatic ligated 1WF origami. (**A**) The influence of various molecules such as ATP (0.5 mM), PNK (20 U) and ligase (2400 U) on the relative migration of the 1WF. (**B**) The effect of proteinase K (10 μg)-treatment on the relative migration of ligated samples. The time-dependent ligation reactions from 0 to 12 h (C) and 12 to 36 h (D). Except the last lane in D) in which 1 mM of ATP was used, in all other lanes, 0.5 mM of ATP was used for ligation reaction. [Ligase] = 2400 U; ligation reaction time = overnight (for **A** & **B**); ligation temperature = 37°C (for **A**, **C** & **D**).

tion in ligation efficiency for a nicked circular DNA at elevated temperatures above 37ºC supports our observations (46). Note that the ligation temperature of 4°C is often used for the blunt end ligation, 16°C is often recommended by the commercial vendors to make sure that the ligase is in active form, and RT ligation is often used for a quick ligation reaction. The reason for the faster migration of the ligated 1WF when compared to the native 1WF is hard to explain at this stage. However, once the detailed analyses are carried out on all four origami structures listed in Figure 1A, a clear picture of the ligation-induced structural changes in the origami and its influence on the relative migration in AGE can be obtained. This is explained in detail at the later stage of this article.

Influence of other factors on the relative migration of bands in AGE

The influence of the ATP, PNK and ligase on the relative migration of the 1WF was also analyzed. As shown in Figure 5A, the faster migration was observed only when all these molecules necessary for the ligation are coexisted in the reaction mixture. This clearly indicated that the observed faster migration was only due to the ligation of the nicks in the staples and not due to the mere presence of any of these molecules. Another way to check the effect of DNA binding enzymes such as PNK and ligase on the relative migration of the bands is to treat the samples with Proteinase K which can digest these enzymes. As shown in Figure 5B, the proteinase K-treated 1WF after ligation still migrates faster and the migration is exactly the same for both proteinase K-treated and untreated 1WF after ligation (with ΔR_f of zero). This confirms our interpretation that the enzyme binding is not the reason for the observed faster migration in case of ligated origami. This data further indicated that the migration of native origami had no temperature dependence (R_f is zero for 4–37°C), while ligated origami exhibited strong temperature dependence on the migration in AGE, indicating the relative ligation efficiencies with better ligation at 37°C.

Optimization of ligation time

The time-dependent ligation shown in Figure 5C indicated that the ligation was not completed within 5 h and requires overnight/12 h. The extended period of ligation from 12 to 36 h indicated that the reaction saturates in 12 h and prolonged ligation does not improve the ligation efficiency (Figure 5D). In all the experiments reported so far, double the amount of ATP when compared to the staples was used during the kinase reaction, and a constant amount of 0.5 mM of ATP was used during the ligation reaction, unless otherwise noted. Increasing the amount of ATP to 1 mM seems not improving the efficiency of ligation as the relative migration of the 1WF is nearly the same (R_f of 0.47 versus 0.49) when both 0.5 and 1 mM of ATP were used (third and last lanes in Figure 5D).

Characterization of ligation in Rec, 3WF and 5WF

Next, we have analyzed the UV-melting profiles and the relative migration patterns in AGE of the native and ligated Rec, 3WF and 5WF origami. Due to the same number and nearly the same length distribution of the staple strands (Figure 1B), the native Rec origami exhibited similar melting profile with that of the 1WF. The melting started at ∼57°C and saturated at ∼80°C, and melting temperatures for the two phases were roughly estimated to be ∼61.5 and ∼65°C. As in the case of 1WF, the hypochromicity was observed for the ligated samples, and the estimated hypochromicity percentages are given below the UV-melting curves (Figure 6A). The maximum hypochromicity was observed at ∼81°C, and the highest difference of ∼38% was observed for the ligation temperature of 37°C. Since the 3WF and 5WF contains relatively longer staple strands and the length distribution of the staples is much wider than Rec and 1WF, the melting patterns observed for the former two origami were somewhat different from the latter two. The melting transitions were not so sharp for 3WF and 5WF and the absorbance at the saturation above 80°C decreased even for the native 3WF and 5WF when compared to Rec (Figure 6A–C). This indicates that

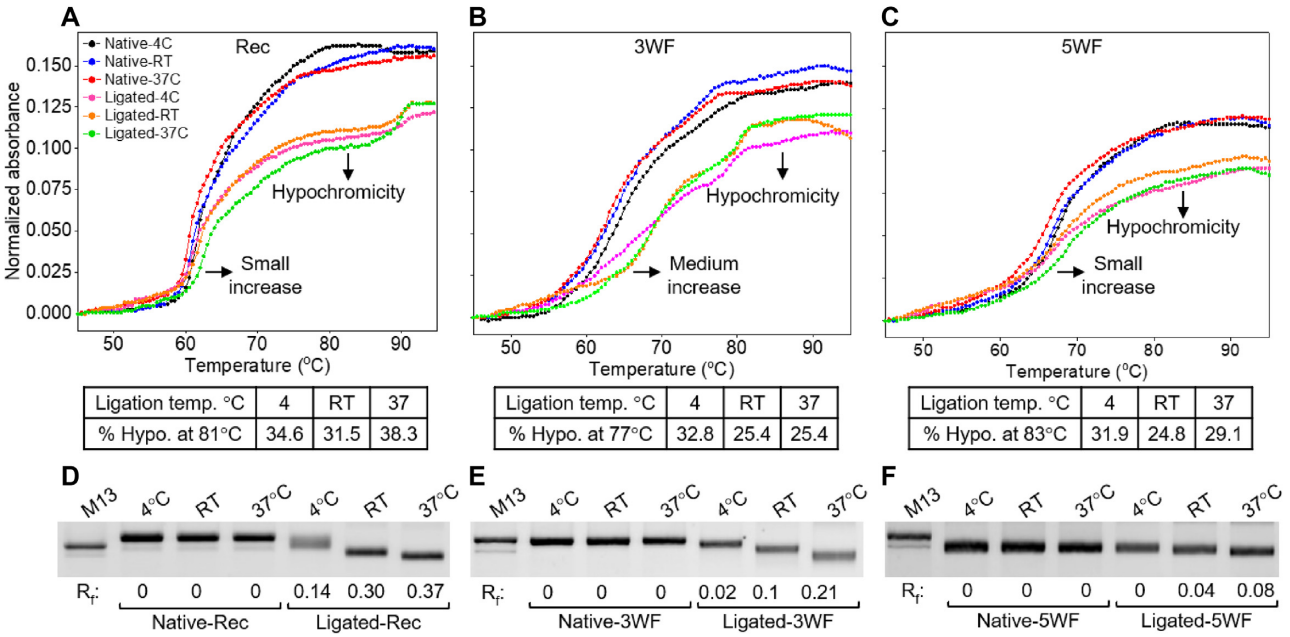

Figure 6. UV-melting analysis (top panel) and native AGE (bottom panel) of the native and ligated Rec (**A**, **D**), 3WF (**B**, **E**) and 5WF (**C**, **F**) origami. The y-axis label and the colour schemes are the same for A-C. [Ligase] = 2400 U; ligation reaction time = overnight; [Origami] = 4 nM (UV-melting) and 3 nM (AGE).

the duplexes of longer staples in native 3WF (up to 64 bp) and 5WF (up to 72 bp) do not melt easily. Though in all the cases the hypochromicity was observed for the ligated samples, the effect is decreasing in the order of 1WF ≈ Rec > 3WF ≈ 5WF. Notably, the 3WF and 5WF samples ligated at 37°C exhibited a slightly lower hypochromicity when compared to 4°C. The observed differences fall within the sensitivity of the UV–visible spectrophotometer, and when this experiment was repeated we could find the maximum hypochromicity for the ligation temperature of 37°C (Supplementary Figure S7D).

The AGE images with estimated R_f values are given below each UV-melting curve (Figure 6D-F). The native Rec origami migrates slower than the M13 which is quite similar to the migration of the 1WF. The native 3WF migrates almost the same speed with that of M13, while it is faster than M13 for the native 5WF. This observation clearly indicates that the relative migration of different types of origami correlates well with the length of the staple strands with slow migration observed for the shorter staples. The same pattern of migration was also reflected in the ligated samples, as the ligation leads to the longer staples that in turn lead to the faster migration of the origami. Another interesting observation is that the relative migration upon ligation was not increased significantly for 5WF (the maximum obtained R_f value was only 0.08), whereas for Rec (R_f of up to 0.37) and 1WF (R_f of up to 0.55, Figure 3F) it was increased drastically. The 3WF exhibited moderate migration with R_f value of up to 0.21. The staple strands are already longer enough to induce the structural changes, such as rigidity and compactness, in 5WF, and thus, it migrates faster than the M13. The ligation of these staples into further longer staples does not influence the structure much, and thus, the R_f value is not increased so much.

Gel mobility shift of all the native and ligated origami

To better understand the relative migration, all the four origami before and after ligation were ran in a single AGE (Figure 7A, top panel). Even in the absence of ligation, different origami structures had different migrations under the same conditions with the R_f values in the order of 5WF > 3WF > 1WF = Rec. The native origami with longer staples migrated faster. The ligation results in further longer staples, and thus, the ligated structures migrated faster than the respective native origami. Further, once ligated, all the origami migrated with similar R_f values (0.49–0.57). This indicates that once ligated, all the origami possibly attain a very similar, rigid and compact globular structure, and thus, they all migrate with similar R_f values.

Effect of EtBr on the migration of native and ligated origami

Unless otherwise stated, all the AGE images presented in this article were recorded after running the EtBr-free gel and then staining with EtBr. When the intercalator EtBr is added to the gel and running buffer during the separation of DNA fragments by AGE, the relative migration of the DNA fragments changes, because it changes the charge, weight, conformation, and flexibility of DNA molecules (47). Thus, to see such a difference in the relative migration of all the four origami before and after ligation, AGE experiment was also carried out in the presence of EtBr both in the gel and running buffer. As shown in Figure 7A, bottom panel, the relative migration of the bands was significantly different when the samples were analyzed using EtBr-containing gel. Even in the absence of ligation, the native origami had quite different migration in the EtBr-containing gel when compared to the EtBr-free gel. Though the migration of native Rec is almost insensitive to the presence of EtBr, all other

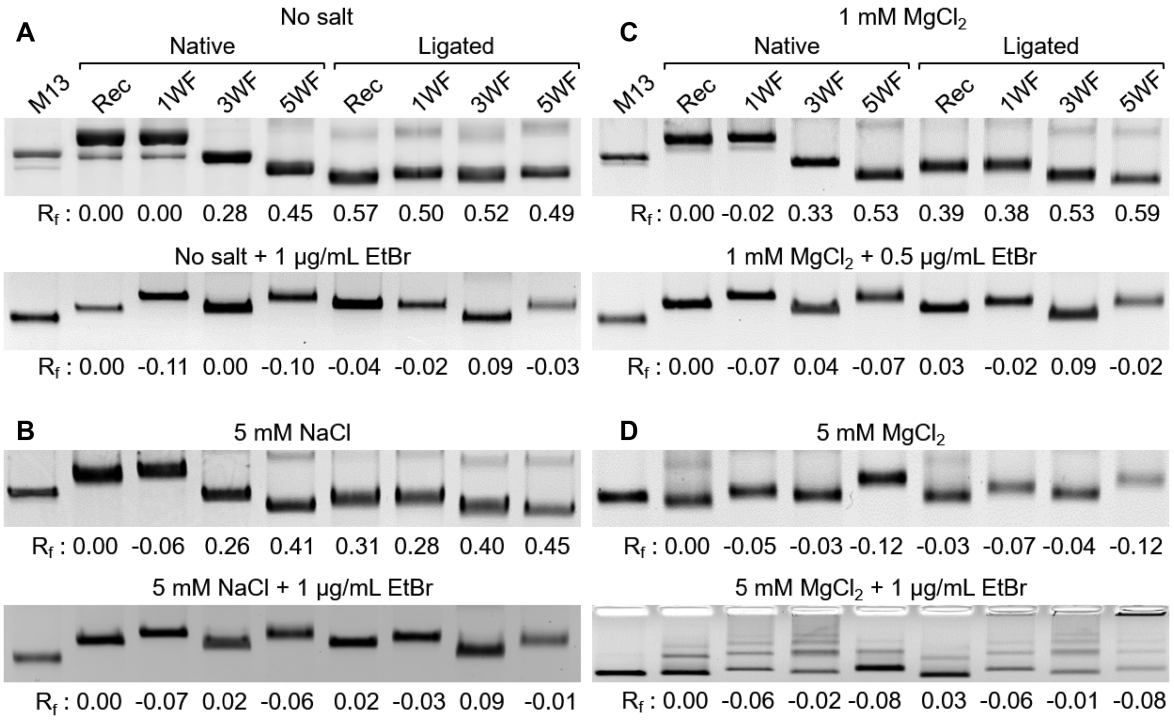

Figure 7. Native AGE images of the non-ligated and enzymatic ligated origami. The gel and running buffer contained no salt (**A**), 5 mM NaCl (**B**), 1 mM $MgCl_2$ (**C**) and 5 mM $MgCl_2$ (**D**). The gel and running buffer contained salt only (top panel), or salt and EtBr (bottom panel). For each lane in the bottom right image, only the R_f value of the fastest migrating band is presented. [Ligase] = 2400 U; ligation reaction time = overnight; ligation temperature = 37°C.

native origami migrated notably slower than in the EtBr-free gel. The relative migration of the native origami and the R_f values followed the order Rec = 3WF > 1WF = 5WF. The ligated origami also exhibited such a slow migration with the R_f in the order of 3WF > Rec = 1WF = 5WF. These observations indicated that the EtBr-binding to the origami significantly alters the globular structure, conformational rigidity/flexibility, and the size of the origami.

Influence of charge of cationic EtBr

In order to further confirm whether EtBr-binding alters the globular structure of the origami or it is the charge of the cationic EtBr which alters the origami migration in AGE, similar experiments were also carried out by adding NaCl or $MgCl_2$ in both gel and running buffer. It is because the effect of charge of cationic EtBr may become negligible in agarose gel containing Na^+ or Mg^{2+}. In the presence of 5 mM NaCl (Figure 7B) or 1 mM $MgCl_2$ (Figure 7C), though minor differences in the band migration were observed, the relative migration of the bands resembled with the one observed in the absence of any salt. Likewise, irrespective of the absence or presence of salts, the band migrations were quite similar for the EtBr-containing gels (Supplementary Figure S8). Thus, eliminating the effect of EtBr charge and confirming our predictions that it is the effect of EtBr intercalation which changes the globular structure of the origami. It is noteworthy that the band migrations were notably different when we used 5 mM $MgCl_2$. Particularly, the simultaneous presence of 5 mM $MgCl_2$ and 1 μg/ml EtBr resulted in the bands that correspond to mono-, di-, tri-, tetra- and even multi-mer (Figure 7D, bottom image). Since higher amount of Mg^{2+} is known to facilitate the formation of higher molecular weight origami (48), this condition is not suitable to distinguish the effect of EtBr intercalation on the globular structure of origami vs the charge of the EtBr on the band migration in AGE.

EtBr concentration-dependent structural changes

One additional factor needs to be confirmed is the EtBr concentration-dependent conformational changes in both native and ligated origami. A constant amount of 3 nM of origami was titrated with increasing amount of EtBr. Two concentration ranges of EtBr were chosen, i.e. one in the low concentration range of 0.2 to 2 μM (Figure 8A-B, left images) and another from 2 to 100 μM (Figure 8A-B, right images). As shown in Figure 8A, the native 1WF migrated faster for the EtBr concentration of 0 to 6 μM, then the bands started to migrate slower until 40 μM of EtBr. From 40 to 100 μM, the bands migrated again slightly faster. As can be seen from Figure 8B-C, similar conformational changes were also observed for the ligated origami, except that a slight decrease in the band migration was initially observed until 1.2 μM of EtBr. After such a concentration, the similar conformational changes with that of the native 1WF were seen for the ligated 1WF. For the EtBr concentration of 1.4–4 μM, the bands migrated faster, from 4 to 40 μM the bands migrated slower, and finally slight increase in band migration was observed above 40 until the maximum tested concentration of 100 μM. These observations clearly

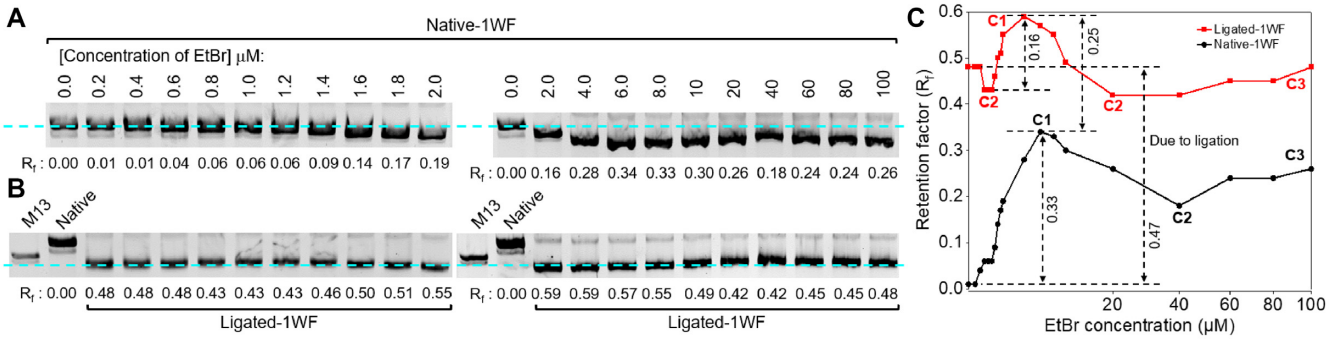

Figure 8. Native AGE images of the EtBr concentration-dependent dynamic and progressive changes in conformation of (**A**) native and (**B**) ligated 1WF. The dotted cyan lines are drawn to indicate the relative migration of the bands. (**C**) The plot of the EtBr concentration vs the retention factor. The three different conformers are indicated by C1, C2 and C3.

indicate that the EtBr-induced conformational change in origami is concentration-dependent.

Analysis of the length distribution of ligated staples

We then performed the denaturing PAGE to visualize the ligated staples and their length distribution. As shown in Figure 9A, the shorter staple strands (24,32,34,36,40 and 44 nucleotides) of native 1WF origami can be clearly seen. The slowest migrating band near the well is due to the M13 scaffold. Apart from these bands, no other distinct band was observed for the native 1WF. The ligated samples exhibited wider staple distribution with the lengths of 64, 96, 128, 160, 192, 224, 256, 288 and 320 nucleotides. The presence of these longer staples indicated that up to 10 staples were ligated in the origami. Based on the 1WF origami design, theoretically ligation of a minimum of 2 and a maximum of 32 staple strands could be possible. In the denaturing PAGE, the percentage of the ligated bands reflect the ligation yield which was calculated to be 55% for 1WF. Further, the ligation at 37°C seems to be optimum as the longer staples over 200 bases in length were absent when the ligation was carried out at 4°C and RT. As shown in Figure 9B, the denaturing PAGE analysis was also performed using the ^{32}P-labelled staples, and a similar pattern with that of the EtBr stained gel was observed. The extremely fainted slow migrating bands in the sample loading wells in Figure 9B indicated the extremely low amount of staple strands in the wells, which confirms the successful denaturation of the origami. This also confirmed that the slow migrating band in the EtBr stained gel (Figure 9A) is exclusively due to the M13 scaffold. Thus, the estimation of the ligation yields based on the fast migrating bands are reliable. A similar pattern was also observed for Rec, 3WF and 5WF (Supplementary Figure S9). The estimated ligation efficiencies for all the four origami are tabulated in Figure 9C. The best ligation efficiencies were obtained when the ligation was performed at 37°C. The PAGE analysis of the time-dependent ligation reactions indicated that overnight reaction yields better ligation efficiency (Supplementary Figure S10). The ligation efficiency followed the order 1WF > Rec > 5WF > 3WF, indicating that there is no significant relationship between the number of wells in the origami and ligation yield. Ligation yields of the 3WF and 5WF might be underestimated as some of the ligated and native staples overlap in the PAGE. Further, we hypothesize that the ligation might be saturated due to the ligation-induced structural changes in the origami rather than the restricted access of the enzyme to the nicks. Besides, the ligation efficiency of 55% is reasonable as the ligation efficiencies reported for the short DNA tiles with only five nicks were as low as 46% and as high as 85% (in average 68 to 77%) (26). In fact, out of the five nicks in that DNA tile, only the four corner nicks were ligated, and the core nick was unable to ligate.

Evaluation of the thermal stability of ligated origami by AFM

Finally, the melting patterns of all the native and ligated origami were investigated by using AFM (Figure 10 and Supplementary Figures S11–S14). The significant results were obtained with the 5WF in which the native origami retained the well-folded structure only until 40°C and started to show visual damages at 45°C (Figure 10B). Though the folded topology and the duplex structures of the origami were seen until 60°C, increasing temperature resulted in the increase in damage. At 65°C, most of the anti-parallel duplex assembly was lost and the 5WF melted almost completely after this temperature. Surprisingly, the ligated 5WF retained the well-folded structure until 60°C, started to show major damage in the topology at 65°C, retained some duplex assembly until 80°C, and melted almost completely after this temperature. The estimated increase in melting point (ΔT_m) for 5WF after ligation was 20°C. Similar results were also observed for other origami and the estimated ΔT_m was 5°C for both Rec and 3WF, and 10°C for 1WF (Figure 10 and Supplementary Figures S11–S13).

DISCUSSIONS

Phosphorylation

In a previous study, incomplete phosphorylation was hypothetically reasoned for the incomplete ligation of DNA nanotubes (26). However, our studies clearly indicated that the phosphorylation goes completion and is not the reason for the incomplete ligation. Alternatively, optimization of the conditions leads to the complete phosphorylation of the staple strands in our case, while such an optimization was not carried out in the previous study.

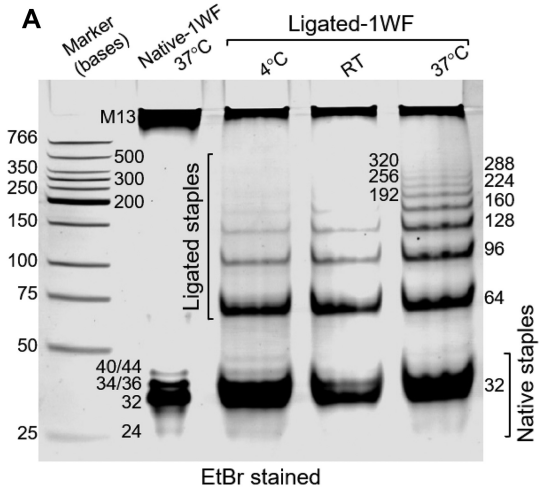

C

Structure	Temp.	Ligation yield (%) EtBr	32P
Rec	4°C	38	
	RT	40	
	37°C	44	45
1WF	4°C	45	
	RT	47	
	37°C	55	52
3WF	4°C	34	
	RT	23	
	37°C	31	38
5WF	4°C	23	
	RT	32	
	37°C	41	44

Figure 9. Denaturing PAGE analysis of the native and ligated 1WF. (**A**) EtBr stained and (**B**) ^{32}P-labelled. The enzymatic ligation was carried out at 4°C, RT and 37°C. The numbers in the image indicate the length of the marker (left most lane) or staple strands. [Ligase] = 2400 U; ligation reaction time = overnight. (**C**) The estimated ligation yields are tabulated.

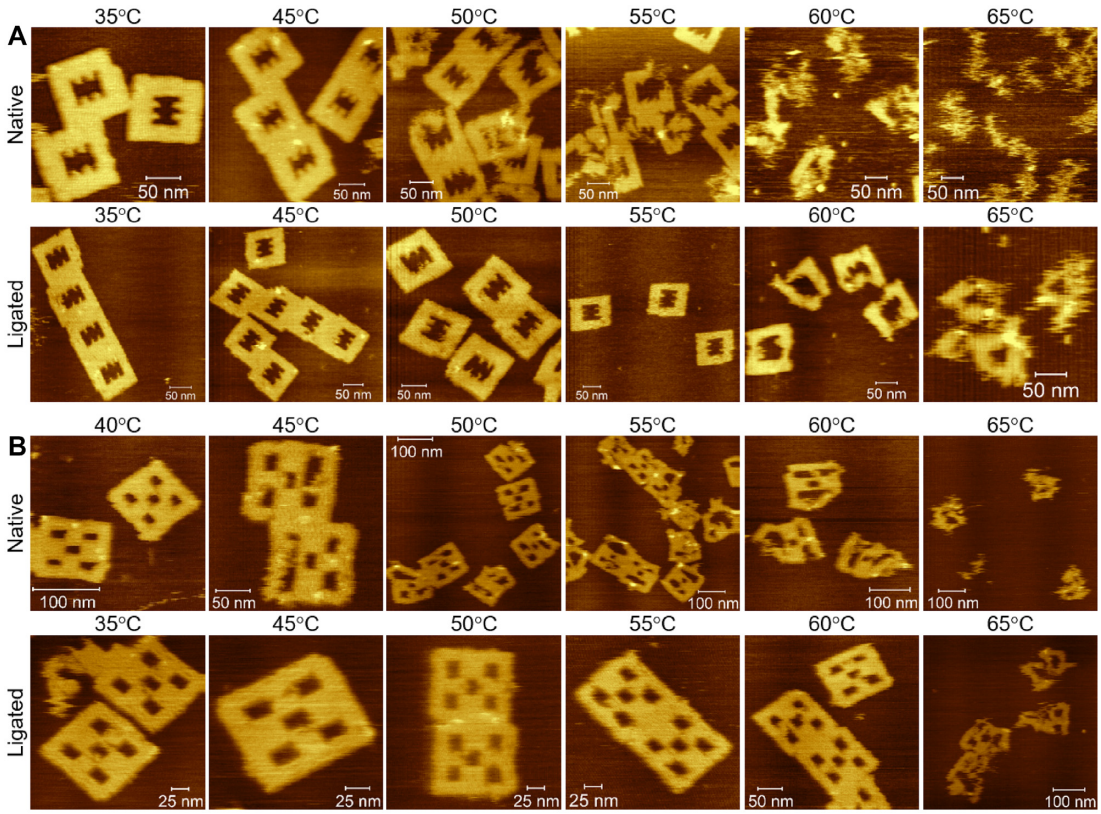

Figure 10. Representative AFM images of the native and enzymatic ligated 1WF (**A**), and 5WF (**B**). [Ligase] = 2400 U; ligation temperature = 37°C; ligation reaction time = overnight; and AFM imaging buffer = 1× origami buffer, pH 8.2.

Ligation-induced structural changes in origami

From the observations in Figure 7A, we can imagine the structural changes in origami when the staple length is increased by ligation, and also when we go from shorter (around 32-mer) to longer (72-mer or above) staples in native origami. The faster migration of the ligated origami when compared to the native origami band indicates the structural changes in the ligated origami into relatively a compact form. Though the presented data alone are insufficient to predict the exact structural changes, we anticipate that the possible structural changes could be the twisting or the self-folding along helical side into a tube-like conformation or it could be even the combination of multiple structural changes. For simplicity, we adopt the model of

twisting along the helical side to explain the compact and rigid form of the ligated origami. Our hypothesis is also supported by the structural design of the origami, as discussed below.

Here, the design of the origami leads to a crossover periodicity of 10.67 bp/helical turn, while it is 10.5 bp/turn in a native B-form DNA. This periodicity leads to an extra 0.5 bp/3 turn in origami which will lead to a twist of ∼17°/3 turn (or 5.7°/turn). Thus, the design by itself may impose a minor twist to the duplexes in the DNA origami. Increasing the staple length from 32 bases to 64, 96, 128 bases, and so on will not change the crossover periodicity. However, ligation of the staple nicks could significantly alter the inter-helical gap between two staple crossover points in a DNA origami (Figure 11A). At the crossover points, the duplexes are in close proximity, while in between the two crossovers, the duplexes are relatively far. This leads to a wider inter-helical gap with relatively flexible duplexes in the non-ligated origami. Once the staple nicks are ligated, a near uniform inter-helical gap is anticipated, which may lead to a tight and compact duplex arrangement with shorter inter-helical distance. This in turn is expected to change the globular structure of the origami, for example, a twist along helical side as graphically depicted in Figure 11B. This ultimately leads to the faster migration of the ligated origami in AGE. Since the faster migration is due to the increased length of the staples, the native 3WF and 5WF with longer staples migrate faster than the native Rec and 1WF that have shorter staples (Figure 7A, top panel).

EtBr-induced static changes in origami structure

The relatively faster migration of the ligated origami when compared to the native origami is reverted by the addition of EtBr in both gel and running buffer (Figure 7A, bottom image). The intercalator EtBr is known to unwind the duplexes by 26° per intercalation (49). Such an unwinding will expand the duplexes along the helical axis and will lead to an elongated origami, as schematically explained in Figure 11C. This elongation along with possible structural change in reverse direction may compensate the above-mentioned structural compactness that was originated from the ligation of the staples and also from the origami design. In this way, the EtBr-bound structure will return to the size which is quite comparable to the native origami, as observed in the AGE (Figure 7). The effect of cationic charge of EtBr on the relative migration of the origami is ruled out as the migration patterns were quite similar when EtBr containing gel and running buffer were supplemented with the mono or divalent metal cations. The observations in Figure 7A further indicates that the staple-length or ligation-dependent changes in globular structure are reversed by the EtBr-binding, while a small difference in the relative migration observed is mainly governed by the relative dimensions of the origami (Figure 1A). The width of the 3WF is the shortest (∼76 nm) among all the four origami, and thus, both native and ligated 3WF still exhibit slightly faster migration than other origami. The 1WF and 5WF occupy relatively a larger volume due to the presence of the wells, and thus migrate slower.

Dynamic and progressive nature of EtBr-induced changes in origami structure

In addition to the static changes in origami conformation, the dynamic and progressive nature of the structural changes were observed by EtBr-concentration dependent AGE analysis. Interestingly, the dynamics of the twisting was observed in a previous study by EtBr or *meso*-tetra(*N*-methyl-4-pyridyl)porphine (TMPyP4) intercalation to a polymerized ribbon and an origami shaft with two flags (50). In this study, the origami design-induced twist was reverted by the EtBr-binding leading to a planar origami. Further, the presence of excess amount of intercalator was reported to over-compensate the origami and lead to the twist in the opposite direction. By considering this previous report and present observations, we characterize that the structural changes lead to three conformers (Figures 8C and 11D). At first, let's consider the native origami in which the initial faster migrating bands are due to the formation of conformer-1 (C1). The EtBr intercalation will expand the size of the origami along the helical axis and it supposed to retard the origami migration in AGE. In contrast to our expectation, the observed faster migration indicates that the EtBr-bound origami may also adopt compact structure possibly by twisting (Figure 11C). Since faster migration was also observed by the ligation, the direction of the structural change in C1 and ligated origami might be the same (twist towards bottom with respect to the plane of origami). Because the conformer-2 (C2) migrates slower, the initial structural change might be reversed, and the origami becomes relatively planar and flexible in this conformer. The structural change seems to be saturating at 40 μM of EtBr, while further increase in the amount of EtBr results in a slight conformational change possibly in the opposite direction (above the plane of origami) and leads to the conformer-3 (C3). As we have observed similar patterns in the ligated bands, the above-mentioned conformational changes and the formation of three different conformers might be the same even for the ligated origami. One exception observed with the ligated origami was the slightly slow migrating band at the initial concentration range of 0.2–1.4 μM of EtBr. At this low concentration range, the origami might have slightly reversed its conformation and approaching towards C2. Note that the EtBr-induced static structural changes observed in Figure 7 resembles the one in C2. Interestingly, the change in band migrations and R_f values are more abrupt for the native origami than the ligated one with a factor of 2.1 (calculated from the maximum differences in R_f, Figure 8C). This indicates that the native origami is more flexible and readily undergoes conformational change while the ligated one is rigid and relatively reluctant for such a conformational change induced by EtBr. Alternatively, the EtBr intercalation is relatively weak for the ligated origami when compared to the non-ligated native one. The possible reasons for this could be the compact structure of the ligated origami, reduced inter-helical gap, and reluctant for the unwinding caused by EtBr intercalation. Because of this weak intercalation, the conformational changes may not be so abrupt when compared to the native origami. This interpretation is well supported by our AGE analysis in which the ligated origami often exhib-

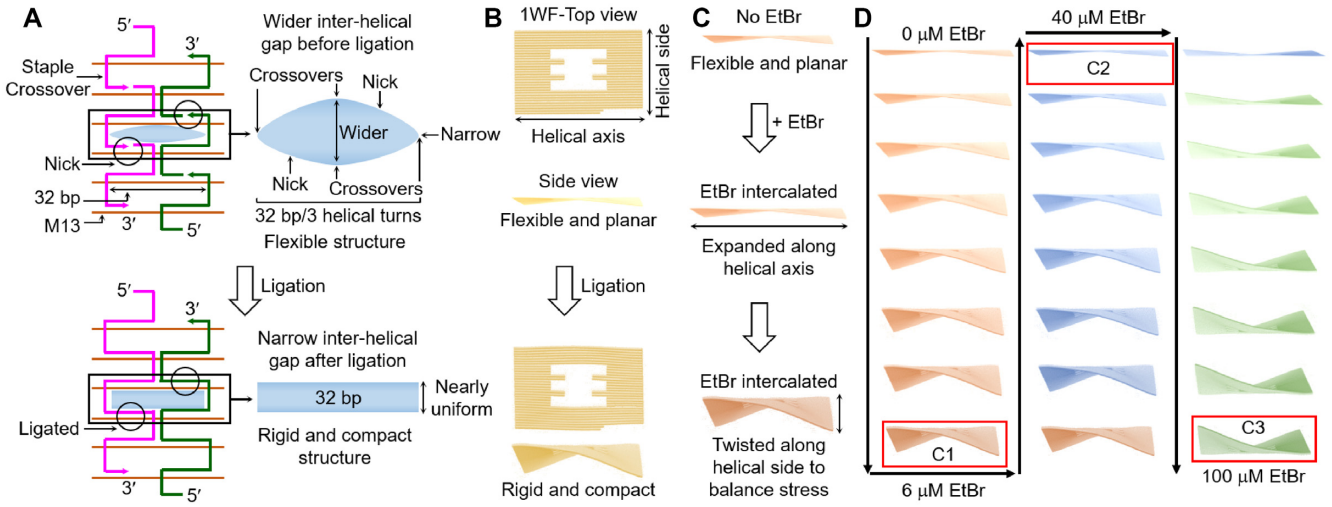

Figure 11. (**A**) Schematic explanation of the inter-helical gap between two staple crossover points in a DNA origami. Top: before ligation, and bottom: after ligation. (**B**) Graphical outline of the possible structural changes in 1WF when the staples are ligated. (**C**) The EtBr intercalation-induced structural elongation along the helical axis and further twisting of the 1WF origami along the helical side are graphically depicted. (**D**) Schematic outline of the EtBr concentration-dependent dynamic and progressive conformational changes in 1WF. Images are not drawn to scale.

ited weak EtBr fluorescence (used for staining the gel) than the native one under similar conditions (see Figures 3D, 5B and 6D–F). Note that the EtBr intercalation-induced origami elongation along helical axis seems to be not a dominant factor in the relative migration of the origami in AGE, while the twisting or structural folding seems to influence strongly. The alternative reason of the twisting itself caused by the origami elongation in case of EtBr binding is unignorable. Apart from these observations, more detailed structural analyses are necessary to unravel the actual structural changes in 2D DNA origami.

The effect of intercalators, such as EtBr, 9-aminoacridine, proflavine, doxorubicin, and PEG-tris-acridine, during the multilayer DNA origami folding on the assembly yield was previously investigated (51). In this study, the measured lengths of the EtBr-bound origami were longer (2–18 nm depending on the origami design) than the expected lengths of EtBr-free origami. This supports our interpretation on the change in globular structure caused by EtBr, the relative sizes of the native, ligated, and EtBr-bound origami, and also the trends in Figure 7. In another study, the EtBr and SYBR Green I-induced twisting was reported for a 420 nm long origami that included two independent six-helix bundles linked together by nine double crossovers (52). In contrast to our observation that the ligation-induced twist is reversed by the EtBr binding, the reported twist in this case was unidirectional and no reversal of the twist was observed. This could be possibly due to the longer length of the six-helix bundles and different design of the origami, i.e. honeycomb in the previous study vs square lattice in our case. One significant difference between the previous studies and the current report is the direction of the changes in origami that leads to the globular twist. In the previous studies, the crossover periodicity along the helical axis (defined as x-axis) induced the globular twist to the origami, whereas in our case, the ligation leads to the change in the staple length and the inter-helical gap along the helical side (y-axis) which resulted the globular twist.

The change in globular structure of the origami was also reported previously for the rectangular origami when anchored onto substrates under a localized electric field (40,41). It is worth mentioning here that when a ligated rectangle origami was used to encapsulate a virus CP, the origami was bent into a tube-like conformation (38). When the ratio of CP to origami was increased, the origami folded further, and a round and chunky complex was observed. The CP binding to the origami was reasoned exclusively for the observed folded structure. However, our current study indicates that we cannot ignore the structural changes in origami induced by the staple ligation. Thus, ignoring such a fundamental investigation will lead to a misinterpretation of the results at least to some extent. Further, our prediction of change in globular structure is supported by a previous study in which the change in global twist of a single-layer rectangular origami of different crossover periodicities (10.44, 10.55 and 10.66 bp/turn) was investigated by small-angle X-ray scattering (SAXS) (53). This study indicated that the origami with crossover periodicity of 10.55 bp/turn is nearly planar, while a slight change in crossover periodicity to 10.44 or 10.66 bp/turn leads to a global twist of 180°. Though, in our case, the ligation of the staples does not change the crossover periodicity, the ligation-induced change in inter-helical gap leads to a similar global twist to the single-layered DNA origami. Our studies further indicate that a simple native AGE analysis provides an extent of such an information on structural changes in DNA origami which parallels to the results obtained by sophisticated techniques such as SAXS.

The change in globular conformation of origami was also reported by the UVB and UVC treatment for the irradiation doses of 6.8 and 2.5 kJ/m^2, respectively, while increasing the doses about 3 times led to the visible defect to the DNA

origami structures (32). In contrast, the origami conformation was shown to be insensitive to UVA treatment, while when combined with a suitable photo-responsible molecule the conformational transition was achieved. One problem with this conformational trigger is the UV light-induced formation of DNA lesions, leading to a non-native DNA structure.

In a previous study using scaffold-free DNA tetrahedron with 20 bp edges, the restriction reaction of DdeI was carried out on both the non-ligated and ligated nanostructures (54). In this case, the ligated structure exhibited increased resistance to the restriction digestion when compared to the non-ligated structure in a position-dependent manner. This report predicted that the overall rigidity of the tetrahedron increases following ligation which strongly supports our interpretation on the ligation-induced structural changes. The restriction reactions on the ligated full-length DNA origami would provide more insights on the ligation-induced structural changes and such an investigation is underway.

Enhanced thermal stability of ligated origami

The enzymatic ligation of the origami improves the melting point about 5–20°C depending on the structure of the origami. By considering the maximum ligation efficiency of ∼55%, the stabilization of 5–10°C is reasonable. The higher stabilization of 20°C observed for 5WF could be possibly due to the lower stability of the native structure, particularly near the wells. Further, this stabilization is interpreted in terms of significant visual damages in the structure rather than the complete collapse of the folded topology, because the folded structures could be seen for the native origami even until 55–60°C. In contrast, due to the absence of wells, the Rec origami is already stable enough and exhibits only slight improvement in the melting point upon ligation. Due to the presence of a large well, the 1WF exhibits moderate stabilization of 10°C which lies in between the Rec and 5WF. Overall, enzymatic ligation of the origami leads to a moderate stabilization when compared to the photo-cross-linking with 8-MOP that increased the melting point ∼30°C (25). The UV-light induced CPD formation method stabilizes the 3D origami up to 90°C (ΔT_m of ∼40°C) (29). The enzymatic ligation performed previously on a 2D triangular origami resulted in a thermal stability of ∼8°C under denaturing conditions with 6 M urea, while no studies were reported on the native conditions after ligation (37).

In the AFM images of the ligated origami, images suggesting the structural changes illustrated in Figure 11B have not been observed. Also, the estimated dimensions of the 1WF origami from the AFM images before and after ligation are quite similar (Supplementary Figure S15). Hence, we anticipate that the structural changes happen only in the solution-state that are well reflected in the AGE analysis. However, when deposited on mica for AFM analysis, the origami structures might be forced to stay planar because of the charged interactions between the negatively charged origami-Mg^{2+}-negatively charged mica and the actual globular structure/topology change was not observed. Our finding is corroborated with the previous studies in which the structural changes such as global twist (53) and curling (55) of origami were unable to probe using AFM.

Structural features of DNA origami from the mechanistic aspect of ligase reaction

The previous reports on the crystal structure of T4 DNA ligase indicated that the enzyme consists of three structural domains namely the N-terminal DNA-binding domain (DBD), nucleotidyl-transferase (NTase) domain, and oligonucleotide-binding (OB-fold) domain (42). The NTase and OBD constitute the catalytic core of this enzyme. The three domains are connected through short linkers and the entire enzyme wraps around the nicked DNA substrate with C-shaped protein clamp. In this binding assembly, each of the domains positioned primarily over the minor groove of the substrate DNA, making the extensive backbone contacts. A salt bridge between Lys384 of OBD and Asp112 of DBD completes the encircling of substrate DNA by T4 DNA ligase (42). By considering these structural features, the NTase-OBD catalytic core and the DBD would bind roughly on the opposite surfaces of the DNA. On the 2D DNA origami this would lead the catalytic core to bind on the top surface and the DBD on the bottom surface of the origami, or vice versa. However, due to the tightly packed anti-parallelly oriented assembly of multiple duplexes, such a binding pattern is unlikely in DNA origami. Thus, the cooperativity between the catalytic core and DBD, and the complete DNA wrapping through C-shaped protein clamp and salt bridge would be lost on the DNA origami. This in turn may force the two domains to interact with the origami individually. If the DBD alone interacts on one surface of the origami, the catalytic reaction would be lost significantly; alternatively, if the catalytic core alone interacts on the other surface, the binding affinity of the ligase to the substrate would be low. This ultimately demands higher amount (2400 U) of the ligase and longer reaction time (overnight) for sealing the staple nicks in DNA origami, as we have observed. The NTase-OBD catalytic core was shown to bind nicked DNA with higher binding affinity (K_d) of 23 μM than the isolated DBD with the K_d of 138 μM (42). This indicates that the enzyme can still bind to the nicked DNA with fair affinity even when the DBD is not effectively interacting with the DNA. As shown previously (42,56), during the course of the nick ligation, the initially adenylated catalytic core of the enzyme forms covalent intermediate through a pyrophosphate linkage between the adenylated enzyme and 5′-phosphate of the nick site. This could be another reason for the binding of the enzyme with fair affinity to the nicked DNA even when the DBD is unable to bind effectively and provide additional binding affinity.

The better ligation efficiency at a relatively higher temperature of 37°C, indicates that the duplexes in the origami slightly open up to conveniently accommodate the enzyme, or more specifically the catalytic core, at the nick site. The alternative reason of the enzyme having its maximum activity at 37°C could not be ignored (46). Besides, a detailed analysis on the correlation of origami loosening or the temperature effect on the ligase enzyme to the ligation efficiency is needed to fully understand the mechanism of temperature dependency (57).

If the enzyme binding to the nick site is not significantly restricted by the tightly packed arrangement of DNA

origami, then the ligation reaction can proceed without further difficulties. Therefore, the enzymatic ligation is not inhibited by the structure of the DNA origami. Nevertheless, as the ligation goes on, the origami structure becomes rigid and compact (Figure 11), which may ultimately influence the enzyme binding to the nick site and further ligation reaction. Thus, the ligation reaction saturates at some point and yields moderate reaction efficiency. Further, the enzyme binding to the nicked DNA distorts and deviates the DNA from B-form conformation, slightly underwounds, and bends 16° (42). Such a DNA distortion and bending would be possible in the initial stages of the origami ligation, while the ligation-induced rigid and compact structure may resist any further structural alterations, and thus, the reaction saturates. Another reason for the saturation of the ligase reaction and obtained lower ligation yields could be the heterogeneity of the ligase-origami interactions at different sites. As shown by the reactions of restriction enzymes (58) and DNase I (59) on DNA origami, different sites on origami exhibit different reactivity, indicating that the enzyme-origami interaction is not uniform throughout the structure and strongly depends on the local and global structural features. The coarse-grained molecular dynamic simulations also supported these experimental observations (60). These studies further indicated the influence of the adjacent duplexes on the enzyme-target site interactions, supporting our interpretations in Figure 11A.

Among the various structural features of nicked DNA-T4 ligase interactions, one important aspect is the number of amino acid residues and nucleic acid bases involved in the extensive contacts between the interacting species. There are 55 amino acid residues from all three domains and 18 bp region centered on the nick were shown to involve in the binding event (42). In all the four origami designs used in this work, 8 bp each on both up and down streams of the nick site are continuous, after which the staple crossover comes (Figure 12). This design would allow the enzyme to interact with 16 bp region, which is 1 bp shorter at each end of the nick site when compared to the crystal structure. If we assume that the DBD is not effectively involving in the enzyme binding on origami, then 16 bp may approximate the interactions observed in the crystal structure. The above-mentioned DNA-enzyme contacts were found to occupy a surface area of 2503 Å^2 (42). In the origami design, the length of 16 bp DNA is ∼54.4 Å (length = 16 bp × 3.4 Å/bp = 54.4 Å), thickness of the DNA duplex is ∼20 Å, and the average inter-helical distance at both the sides of a nicked DNA is ∼15 × 2 = 30 Å (width = 20 + 15 + 15 = 50 Å). In such a design, the surface area of ∼2720 Å^2 (area = length × width = 54.4 × 50 = 2720 Å^2) would be theoretically available for the DNA-enzyme contact, which is in close approximation with the dimension estimated from the crystal structure. Hence, the nick site in origami may provide tight but mere sufficient space to accommodate the enzyme, or at least the catalytic core.

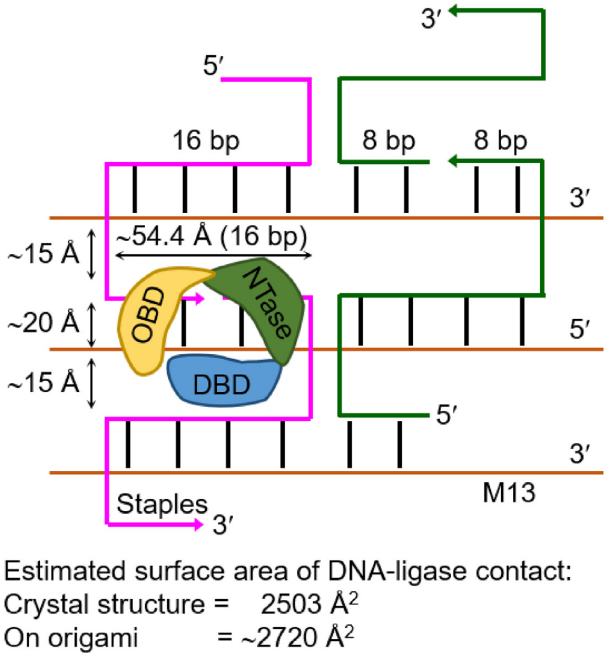

Figure 12. Schematic explanation of the duplex arrangements in a DNA origami and the T4 DNA ligase binding at a nick site. The three domains of the ligase enzyme, and the estimated surface area of the DNA-ligase contact are shown. Image is not drawn to scale.

CONCLUSIONS

The enzymatic ligation of the staple nicks of four different 2D DNA origami was carried out. The UV-melting analysis indicated that the melting point is not a good measure to investigate the enzymatic ligation, while the hypochromicity is a good indication of the ligation. The ligation-induced mobility changes of the origami are well characterized by AGE analysis. The ligated origami with longer staples deviates from the near/moderately planar structure, and adopts rigid and compact topology. This in turn leads to their faster migration in AGE when compared to the non-ligated origami with shorter staples. The conditions for the PNK and T4 DNA ligase reactions were optimized. For a typical origami synthesis of 10–40 nM, double the amount of ATP when compared to the concentration of staples and 10–30 U of PNK are sufficient for a 30 min reaction at 37°C. The ligation reaction takes overnight incubation at 37°C to saturate, and requires 0.5 mM ATP and 2400 U of T4 DNA ligase. Under these optimized conditions, the estimated ligation yields ranged from 38 to 55%. Denaturing PAGE analysis indicated that up to 10 staple strands are ligated under the optimized conditions. The melting analysis carried out by AFM indicated that the ligation increases the melting point of origami about 5 to 20°C, depending on the structure. The dynamic and progressive nature of the conformational change in DNA origami caused by EtBr intercalation are well characterized. Overall, our results are useful to understand the optimized conditions for the enzymatic ligation of DNA origami structures, ligation-induced structural rigidity and compactness, the access of ligase enzyme in a tightly packed environment, and the nature of EtBr binding and its influence on the conformational change in origami.

SUPPLEMENTARY DATA

Supplementary Data are available at NAR Online.

ACKNOWLEDGEMENTS

We acknowledge the kind help of Prof. Takayuki Uchihashi with AFM.

FUNDING

Ministry of Education, Culture, Sports, Science and Technology (MEXT, Japan) for the Grants-in-Aid for Scientific Research [16K17934, 21K05274 to A.R., 19H04653, 20H02860 to E.N., 17H01213 to T.M., JST CREST JPMJCR18H5 to T.M.]; Kyoto University Foundation for the Research Grant [to A.R.]; Institute of Advanced Energy, Kyoto University for the Research Grant for Collaboration Program of the Laboratory for Complex Energy Processes [to A.R.]; MEXT-SGU Scholarship [to K.K.]. Funding for open access charge: Core Research for Evolutional Science and Technology [JPMJCR18H5].
Conflict of interest statement. None declared.

REFERENCES

1. Seeman,N.C. (1982) Nucleic acid junctions and lattices. *J. Theor. Biol.*, **99**, 237–247.
2. Seeman,N.C. (2003) DNA in a material world. *Nature*, **421**, 427–431.
3. Rothemund,P.W.K. (2006) Folding DNA to create nanoscale shapes and patterns. *Nature*, **440**, 297–302.
4. Lund,K., Liu,Y., Lindsay,S. and Yan,H. (2005) Self-assembling a molecular pegboard. *J. Am. Chem. Soc.*, **127**, 17606–17607.
5. Park,S.H., Pistol,C., Ahn,S.J., Reif,J.H., Lebeck,A.R., Dwyer,C. and LaBean,T.H. (2006) Finite-size, fully addressable DNA tile lattices formed by hierarchical assembly procedures. *Angew. Chem. Int. Ed.*, **45**, 735–739.
6. Chworos,A., Severcan,I., Koyfman,A.Y., Weinkam,P., Oroudjev,E., Hansma,H.G. and Jaeger,L. (2004) Building Programmable jigsaw puzzles with RNA. *Science*, **306**, 2068–2072.
7. Kuzuya,A. and Komiyama,M. (2009) Design and construction of a box-shaped 3D-DNA origami. *Chem. Commun.*, **28**, 4182–4184.
8. Ke,Y., Sharma,J., Liu,M., Jahn,K., Liu,Y. and Yan,H. (2009) Scaffolded DNA origami of a DNA tetrahedron molecular container. *Nano Lett.*, **9**, 2445–2447.
9. Douglas,S.M., Dietz,H., Liedl,T., Högberg,B., Graf,F. and Shih,W.M. (2009) Self-assembly of DNA into nanoscale three-dimensional shapes. *Nature*, **459**, 414–418.
10. Rajendran,A., Endo,M., Katsuda,Y., Hidaka,K. and Sugiyama,H. (2011) Programmed two-dimensional self-assembly of multiple DNA origami jigsaw pieces. *ACS Nano*, **5**, 665–671.
11. Endo,M., Sugita,T., Rajendran,A., Katsuda,Y., Emura,T., Hidaka,K. and Sugiyama,H. (2011) Two-dimensional DNA origami assemblies using a four-way connector. *Chem. Commun.*, **47**, 3213–3215.
12. Liu,W., Zhong,H., Wang,R. and Seeman,N.C. (2011) Crystalline two-dimensional DNA-origami arrays. *Angew. Chem. Int. Ed.*, **50**, 264–267.
13. Zhao,Z., Liu,Y. and Yan,H. (2011) Organizing DNA origami tiles into larger structures using preformed scaffold frames. *Nano Lett.*, **11**, 2997–3002.
14. Rajendran,A., Endo,M., Hidaka,K., Shimada,N., Maruyama,A. and Sugiyama,H. (2014) A lock-and-key mechanism for the controllable fabrication of DNA origami structures. *Chem. Commun.*, **50**, 8743–8746.
15. Eskelinen,A.-P., Rosilo,H., Kuzyk,A., Torma,P. and Kostiainen,M.A. (2012) Controlling the formation of DNA origami structures with external signals. *Small*, **8**, 2016–2020.
16. Rajendran,A., Endo,M. and Sugiyama,H. (2012) DNA origami: synthesis and self-assembly. *Curr. Protoc. Nucleic Acid Chem.*, **48**, 12.9.1–12.9.18.
17. Sharma,J., Chhabra,R., Andersen,C.S., Gothelf,K.V., Yan,H. and Liu,Y. (2008) Toward reliable gold nanoparticle patterning on self-assembled DNA nanoscaffold. *J. Am. Chem. Soc.*, **130**, 7820–7821.
18. Ding,B., Deng,Z., Yan,H., Cabrini,S., Zuckermann,R.N. and Bokor,J. (2010) Gold nanoparticle self-similar chain structure organized by DNA origami. *J. Am. Chem. Soc.*, **132**, 3248–3249.
19. Wang,R., Nuckolls,C. and Wind,S.J. (2012) Assembly of heterogeneous functional nanomaterials on DNA origami scaffolds. *Angew. Chem. Int. Ed.*, **51**, 11325–11327.
20. Maune,H.T., Han,S.-P., Barish,R.D., Bockrath,M., Goddard,W.A. III, Rothemund,P.W.K. and Winfree,E. (2010) Self-assembly of carbon nanotubes into two-dimensional geometries using DNA origami templates. *Nat. Nanotechnol.*, **5**, 61–66.
21. Rajendran,A., Nakata,E., Nakano,S. and Morii,T. (2017) Nucleic-acid-templated enzyme cascades. *Chem. Biol. Chem.*, **18**, 696–716.
22. Stephanopoulos,N., Liu,M., Tong,G.J., Li,Z., Liu,Y., Yan,H. and Francis,M.B. (2010) Immobilization and one-dimensional arrangement of virus capsids with nanoscale precision using DNA origami. *Nano Lett.*, **10**, 2714–2720.
23. Udomprasert,A. and Kangsamaksin,T. (2017) DNA origami applications in cancer therapy. *Cancer Sci.*, **108**, 1535–1543.
24. Rajendran,A., Endo,M. and Sugiyama,H. (2012) Single-molecule analysis using DNA origami. *Angew. Chem. Int. Ed.*, **51**, 874–890.
25. Rajendran,A., Endo,M., Katsuda,Y., Hidaka,K. and Sugiyama,H. (2011) Photo-cross-linking-assisted thermal stability of DNA origami structures and its application for higher-temperature self-assembly. *J. Am. Chem. Soc.*, **133**, 14488–14491.
26. O'Neill,P., Rothemund,P.W.K., Kumar,A. and Fygenson,D.K. (2006) Sturdier DNA nanotubes via ligation. *Nano Lett.*, **6**, 1379–1383.
27. Endo,M., Hidaka,K. and Sugiyama,H. (2011) Direct AFM observation of an opening event of a DNA cuboid constructed via a prism structure. *Org. Biomol. Chem.*, **9**, 2075–2077.
28. Rajendran,A., Endo,M. and Sugiyama,H. (2014) State-of-the-art high-speed atomic force microscopy for investigation of single-molecular dynamics of proteins. *Chem. Rev.*, **114**, 1493–1521.
29. Gerling,T., Kube,M., Kick,B. and Dietz,H. (2018) Sequence-programmable covalent bonding of designed DNA assemblies. *Sci. Adv.*, **4**, eaau1157.
30. Ramakrishnan,S., Ijäs,H., Linko,V. and Keller,A. (2018) Structural stability of DNA origami nanostructures under application-specific conditions. *Comput. Struct. Biotechnol. J.*, **16**, 342–349.
31. Bila,H., Kurisinkal,E.E. and Bastings,M.M.C. (2019) Engineering a stable future for DNA-origami as a biomaterial. *Biomater. Sci.*, **7**, 532–541.
32. Chen,H., Li,R., Li,S., Andréasson,J. and Choi,J.H. (2017) Conformational effects of UV light on DNA origami. *J. Am. Chem. Soc.*, **139**, 1380–1383.
33. Mousavi-Khattat,M., Rafati,A. and Gill,P. (2015) Fabrication of DNA nanotubes using origami-based nanostructures with sticky ends. *J. Nanostruct. Chem.*, **5**, 177–183.
34. Yang,X., Wenzler,L.A., Qi,J., Li,X. and Seeman,N.C. (1998) Ligation of DNA triangles containing double crossover molecules. *J. Am. Chem. Soc.*, **120**, 9779–9786.
35. Petrillo,M.L., Newton,C.J., Cunningham,R.P., Ma,R.-I., Kallenbach,N.R. and Seeman,N.C. (1988) The ligation and flexibility of four-arm DNA junctions. *Biopolymers*, **27**, 1337–1352.
36. LaBean,T.H., Yan,H., Kopatsch,J., Liu,F., Winfree,E., Reif,J.H. and Seeman,N.C. (2000) Construction, analysis, ligation, and self-assembly of DNA triple crossover complexes. *J. Am. Chem. Soc.*, **122**, 1848–1860.
37. Ramakrishnan,S., Schärfen,L., Hunold,K., Fricke,S., Grundmeier,G., Schlierf,M., Keller,A. and Krainer,G. (2019) Enhancing the stability of DNA origami nanostructures: staple strand redesign versus enzymatic ligation. *Nanoscale*, **11**, 16270–16276.
38. Mikkilä,J., Eskelinen,A.-P., Niemelä,E.H., Linko,V., Frilander,M.J., Törmä,P. and Kostiainen,M.A. (2014) Virus-encapsulated DNA origami nanostructures for cellular delivery. *Nano Lett.*, **14**, 2196–2200.
39. Eskelinen,A.P., Kuzyk,A., Kaltiaisenaho,T.K., Timmermans,M.Y., Nasibulin,A.G., Kauppinen,E.I. and Törmä,P. (2011) Assembly of single-walled carbon nanotubes on DNA-origami templates through streptavidin-biotin interaction. *Small*, **7**, 746–750.
40. Kuzyk,A., Yurke,B., Toppari,J.J., Linko,V. and Törmä,P. (2008) Dielectrophoretic trapping of DNA origami. *Small*, **4**, 447–450.

41. Linko,V., Paasonen,S.-T., Kuzyk,A., Törmä,P. and Toppari,J.J. (2009) Characterization of the conductance mechanisms of DNA origami by AC impedance spectroscopy. *Small*, **5**, 2382–2386.
42. Shi,K., Bohl,T.E., Park,J., Zasada,A., Malik,S., Banerjee,S., Tran,V., Li,N., Yin,Z., Kurniawan,F. *et al.* (2018) T4 DNA ligase structure reveals a prototypical ATP-dependent ligase with a unique mode of sliding clamp interaction. *Nucleic Acids Res.*, **46**, 10474–10488.
43. Endo,M., Katsuda,Y., Hidaka,K. and Sugiyama,H. (2010) Regulation of DNA methylation using different tensions of double strands constructed in a defined DNA nanostructure. *J. Am. Chem. Soc.*, **132**, 1592–1597.
44. Ngo,T.A., Nakata,E., Saimura,M. and Morii,T. (2016) Spatially organized enzymes drive cofactor-coupled cascade reactions. *J. Am. Chem. Soc.*, **138**, 3012–3021.
45. Nakata,E., Liew,F.F., Uwatoko,C., Kiyonaka,S., Mori,Y., Katsuda,Y., Endo,M., Sugiyama,H. and Morii,T. (2012) Zinc-finger proteins for site-specific protein positioning on DNA-origami structures. *Angew. Chem. Int. Ed.*, **51**, 2421–2424.
46. Phol,F.M., Thomae,R. and Karst,A. (1982) Temperature dependence of the activity of DNA-modifying enzymes: endonucleases and DNA ligase. *Eur. J. Biochem.*, **123**, 141–152.
47. Sigmon,J. and Larcom,L.L. (1996) The effect of ethidium bromide on mobility of DNA fragments in agarose gel electrophoresis. *Electrophoresis*, **17**, 1524–1527.
48. Douglas,S.M., Bachelet,I. and Church,G.M. (2012) A logic-gated nanorobot for targeted transport of molecular payloads. *Science*, **335**, 831–834.
49. Liu,L.F. and Wang,J.C. (1975) On the degree of unwinding of the DNA helix by ethidium: II. Studies by electron microscopy. *Biochim. Biophys. Acta Nucleic Acids Protein Synth.*, **395**, 405–412.
50. Chen,H., Zhang,H., Pan,J., Cha,T.-G., Li,S., Andréasson,J. and Choi,J.H. (2016) Dynamic and progressive control of DNA origami conformation by modulating DNA helicity with chemical adducts. *ACS Nano*, **10**, 4989–4996.
51. Ke,Y., Bellot,G., Voigt,N.V., Fradkov,E. and Shih,W.M. (2012) Two design strategies for enhancement of multilayer–DNA-origami folding: underwinding for specific intercalator rescue and staple-break positioning. *Chem. Sci.*, **3**, 2587–2597.
52. Zadegan,R.M., Lindau,E.G., Klein,W.P., Green,C., Graugnard,E., Yurke,B., Kuang,W. and Hughes,W.L. (2017) Twisting of DNA origami from intercalators. *Sci. Rep.*, **7**, 7382.
53. Baker,M.A.B., Tuckwell,A.J., Berengut,J.F., Bath,J., Benn,F., Duff,A.P., Whitten,A.E., Dunn,K.E., Hynson,R.M., Turberfield,A.J. *et al.* (2018) Dimensions and global twist of single-layer DNA origami measured by small-angle X-ray scattering. *ACS Nano*, **12**, 5791–5799.
54. Keum,J.-W. and Bermudez,H. (2009) Enhanced resistance of DNAnanostructures to enzymatic digestion. *Chem. Commun.*, **45**, 7036–7038.
55. Mallik,L., Dhakal,S., Nichols,J., Mahoney,J., Dosey,A.M., Jiang,S., Sunahara,R.K., Skiniotis,G. and Walter,N.G. (2015) Electron microscopic visualization of protein assemblies on flattened DNA origami. *ACS Nano*, **9**, 7133–7141.
56. Johnson,A. and O'Donnell,M. (2005) DNA ligase: Getting a grip to seal the deal. *Curr. Biol.*, **15**, R90–R92.
57. Suzuki,M., Hayashi,H., Mizuki,T., Maekawa,T. and Morimoto,H. (2016) Efficient DNA ligation by selective heating of DNA ligase with a radio frequency alternating magnetic field. *Biochem. Biophys. Rep.*, **8**, 360–364.
58. Stopar,A., Coral,L., Di,G.S., Adedeji,A.F. and Castronovo,M. (2017) Binary control of enzymatic cleavage of DNA origami by structural antideterminants. *Nucleic Acids Res.*, **46**, 995–1006.
59. Ramakrishnan,S., Shen,B., Kostiainen,M.A., Grundmeier,G., Keller,A. and Linko,V. (2019) Real-time observation of superstructure-dependent DNA origami digestion by DNase I using high-speed atomic force microscopy. *Chem. Biol. Chem.*, **20**, 2818–2823.
60. Suma,A., Stopar,A., Nicholson,A.W., Castronovo,M. and Carnevale,V. (2020) Global and local mechanical properties control endonuclease reactivity of a DNA origami nanostructure. *Nucleic Acids Res.*, **48**, 4672–4680.